Trans Indian Inst Met (2021) 74(7):1603–1609
https://doi.org/10.1007/s12666-021-02252-3

ORIGINAL ARTICLE

Tuning Glass Formation and Mechanical Properties of ZrCoAl(Nb) Bulk Metallic Glass with Nb Microalloying Process

Morteza Mahmoodan[1] · Reza Gholamipour[2] · Sajad Sohrabi[2]

Received: 22 January 2021 / Accepted: 29 March 2021 / Published online: 21 April 2021

Abstract In the present study, the effect of Nb addition on mechanical behavior and glass formation in $(Zr_{56}Co_{28}Al_{16})_{100-x}Nb_{(x=0,2,4)}$ bulk metallic glasses was studied. The differential scanning calorimetry (DSC) was used to investigate thermal properties of samples. Further, mechanical behavior of prepared samples was analyzed using quasi-static compressive tests. The results showed that 2 at.% minor addition of Nb enhances the glass forming ability (GFA), but larger amount of Nb (4%) deteriorates GFA. The X-ray diffraction patterns also confirmed that the structures of whole of studied compositions are amorphous. In addition, the compressive test results revealed that 2% addition of Nb significantly improves compressive ultimate strength (up to 2.5 GPa) and increases the plastic strain from 1.1% in the composition having no Nb content to ~ 6%. The observation of shear band branching and also the increase in the density of vein-like patterns in the fracture surface (studied by scanning electron microscopy) also confirm the improvement of plasticity in $(Zr_{56}Co_{28}Al_{16})_{98}Nb_2$ sample. Our finding highlights the effect of minor alloying on the formation and mechanical properties of bulk metallic glasses.

✉ Morteza Mahmoodan
mahmoodan1981m@gmail.com

✉ Reza Gholamipour
rgholamipour@gmail.com

[1] Department of Materials Science and Engineering, Saveh Branch, Islamic Azad University, Saveh, Iran

[2] Department of Advanced Materials and Renewable Energy, Iranian Research Organization for Science and Technology (IROST), Tehran, Iran

Keywords Bulk metallic glasses · Glass forming ability · Plasticity · Minor alloying · Shear band

1 Introduction

Bulk metallic glasses (BMGs) show excellent mechanical properties such as large elastic limit and giant yield stress, but they frequently fail in a brittle manner during compressive or tensile loading at room temperature. This shortcoming is the major restriction for the development of BMGs as advanced engineering materials [1–5]. In order to extend the application of BMGs and overcome their brittleness, various methods such as thermomechanical processing [6] and the minor addition of alloying elements (microalloying) have been developed. The microalloying strategy enables us to control the glass formation and improve the plasticity of BMGs. Thus, this technique can be used as a suitable way to develop new BMG compositions with high GFA and prominent mechanical properties [7–12].

Zr-based BMGs have been widely used for structural applications in recent decades due to their excellent properties such as high GFA, superior mechanical properties, good corrosion resistance, good biocompatibility, and high wear resistance [13–17]. Among various Zr-based BMGs developed, the ternary Zr–Co–Al alloy system is a good candidate for biomedical applications mainly due to its suitable mechanical properties and also lack of the toxic elements such as Ni and Be [18–21]. While the previous studies on the minor alloying of Zr–Co–Al BMG have mostly focused on improving thermal and biomedical properties, less attention has been so far paid on the enhancement of mechanical properties. For instance, Zhang et al. [22] investigated the influence of Ag addition

on the enhancement of GFA and bio-corrosion resistance in Zr–Co–Al BMG, but the mechanical response of Ag-doped BMG was not reported. In addition, the extent of compressive ultimate strength achieved after minor alloying of Zr–Co–Al BMG is often unsatisfactory. For example, Rahvard et al. [23] studied the effect of substitution of Co by Cu on the thermal and mechanical properties of $Zr_{56}Co_{28-x}Cu_xAl_{16}$ BMG and reported a maximum compressive strength of ~ 2.1 GPa in $Zr_{56}Co_{22}Cu_6Al_{16}$ alloy composition. In the present work, we systematically study the effect of Nb content on the mechanical properties and glass formation in $(Zr_{56}Co_{28}Al_{16})_{100-x}Nb_x$ BMG samples.

2 Materials and Methods

Ingots of $(Zr_{56}Co_{28}Al_{16})_{100-x}Nb_{(x=0,2,4)}$ (at.%) were prepared by arc melting of high-purity elements in Ti-gettered and Ar atmosphere in a water-cooled copper crucible. Here, we denote the compositions containing 0%, 2%, and 4% of Nb as Nb-0, Nb-2, and Nb-4 samples, respectively. Zr and Nb elements were first melted together, and then, other elements were added to the Nb-Zr ingot and remelted several times to form a homogeneous alloy. In the next step, the prepared melted alloy was cast into a water-cooled copper mold to make BMG rods with 2-mm diameter. The structural characterizations of as-cast rods were carried out using an X-ray diffraction (XRD, Bruker D8) instrument with Cu-K_α radiation. In order to prepare samples for compression test, the as-cast rods were cut by a low speed micro-cutter into small cylinders, and then, both sides of each cylinder were polished. The quasi-static compression tests were performed using a SANTAM (STM-250) universal testing machine at a strain rate of 10^{-4} s^{-1}. The gauge dimension of specimens was 2 mm in diameter and 4 mm in height for the compressive test. The thermal behavior of samples was characterized using differential scanning calorimeter (DSC, PerkinElmer STA 6000) at the heating rate of 20 K/min. The microstructural observations on fractured samples after compression test were performed using secondary electron imaging in a field emission scanning electron microscope (FE-SEM, Tescan Mira).

3 Results and Discussion

Figure 1 shows the XRD patterns of the as-cast BMG samples. Since there are no sharp and narrow peaks (as the characteristics of crystalline structures), the structure of prepared samples is amorphous. The only peak observed for all samples is a broad, low-intensity peak occurring at 2θ in the range of 35°–40°, which is a signature of the amorphous nature of structure in this alloy system [19, 20].

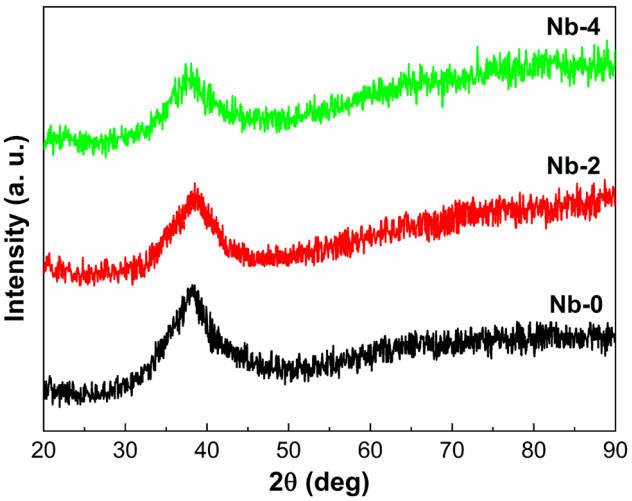

Fig. 1 The XRD patterns of as-cast Nb-0, Nb-2, and Nb-4 samples

Therefore, the addition of Nb even up to 4% would not cause crystallization in the as-cast 2-mm BMG rods.

The DSC signals of the as-cast BMG samples are shown in Fig. 2. By heating up the samples, various physical transitions occur for the as-cast samples, including glass transition, crystallization, and melting. The onset temperature of glass transition (T_g), the onset temperature of crystallization (T_x), the solidus temperature (T_m), and the liquidus temperature (T_L) are determined from DSC curves and summarized in Table 1.

As can be seen from Fig. 2a, the onset temperature of glass transition (T_g) and the onset temperature of crystallization (T_x) decrease monotonically with the increase in the Nb content. In addition, while Nb-0 sample has two overlapped crystallization peaks, Nb-2 and Nb-4 samples have two distinct crystallization peaks. This observation reveals that Nb addition dramatically changes the crystallization behavior of $Zr_{56}Co_{28}Al_{16}$ BMG. Further, it is evident from Fig. 2b that the Nb content decreases the width of the melting transition (i.e., the difference between T_m and T_L).

We have evaluated the GFA of prepared samples using different GFA indicators [1], including the γ parameter ($\gamma = T_x/(T_g + T_L)$), the reduced glass transition temperature ($T_{rg} = T_g/T_L$), the α parameter ($\alpha = (T_x/T_L)$), the δ parameter ($\delta = T_x/(T_L - T_g)$, and *new* β parameter (*new* $\beta = T_x \times T_g/(T_L - T_x)^2$). Further, the thermal stability upon heating from the glassy state is examined by measuring the width of the supercooled liquid region ($\Delta T_x = T_x - T_g$).

The calculated values of the above indicators are given in Table 1. While the γ parameter is almost the same for all samples, the other GFA indicators (T_{rg}, α, *new* β, and δ parameters) show increasing trend in Nb-2 sample. This increasing trend in various GFA parameters denotes that

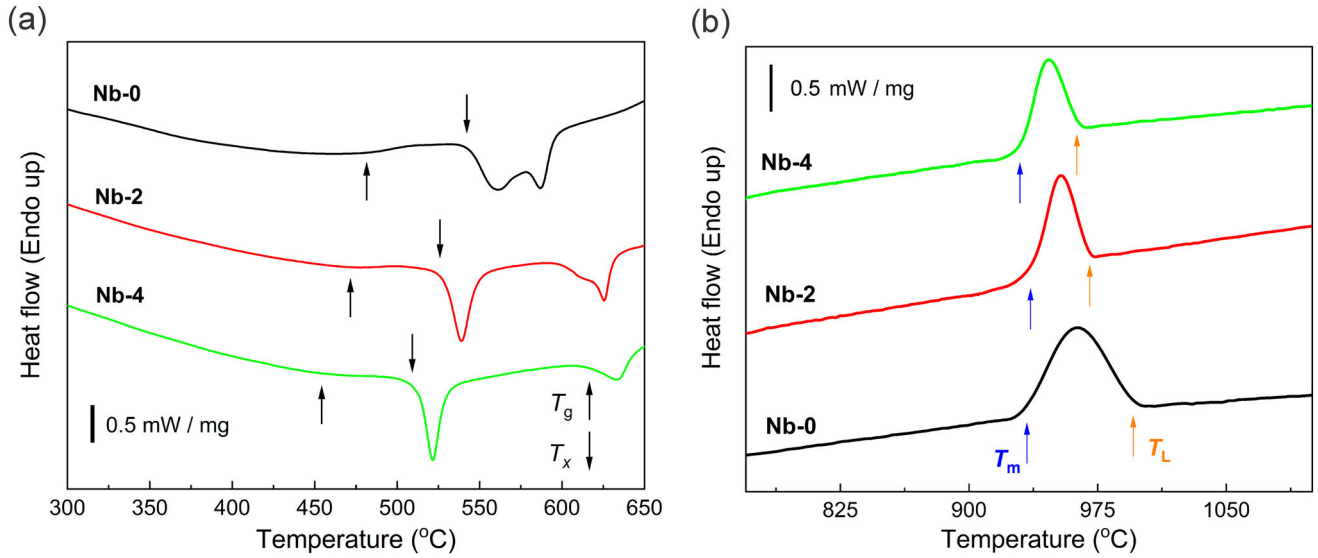

Fig. 2 DSC thermographs of as-cast Nb-0, Nb-2, and Nb-4 samples

Table 1 Thermal properties of Nb-0, Nb-2, and Nb-4 BMG samples. The maximum error for determining T_g, T_x, T_m, and T_L is ± 2 °C

Sample	T_g (°C)	T_x (°C)	T_m (°C)	T_L (°C)	ΔT_x	*Trg*	α	γ	δ	*new* β
Nb-0	480.0	542.8	932.3	1000.12	62.8	0.591	0.640	0.402	1.568	2.937
Nb-2	472.7	528.2	937	971.40	55.5	0.599	0.644	0.402	1.607	3.041
Nb-4	450.3	512.5	930.8	966.20	62.2	0.583	0.634	0.400	1.522	2.760

GFA has improved by adding 2 at.% of Nb. However, adding larger amounts of Nb (4 at.% in Nb-4 sample) sensibly reduces the values of these parameters, suggesting the deterioration of GFA in Nb-4 sample compared to the other samples. Among the studied parameters, the variations in the GFA induced by Nb minor alloying are more evident by considering *new* β and δ parameters. It can be therefore concluded from the data in Table 1 that Nb-2 has the highest GFA among the studied compositions.

In contrast to the GFA, thermal stability upon heating (ΔT_x) decreases in Nb-2 to some extent ($\sim$ 7 °C), but the value in Nb-4 is comparable to that of the Nb-free sample (Nb-0). This implies that during heating, thermal stability of the amorphous state against crystallization is reduced in Nb-2 sample and the processability of this alloy within the supercooled liquid region is slightly decreased. Thus, GFA and thermal stability in the studied compositions are decoupled and show divergent evolutions, as previously observed in Ti–Zr–Cu–S [24] and Zr–Ti–Ni–Cu–Be alloy systems [25].

Various parameters influence the GFA of BMGs, namely type of the atoms and their interactions, the atomic size, and the mixing enthalpy of the constituent elements. The atomic radius for Zr, Co, Al, and Nb is 0.206 nm, 0.152 nm, 0.118 nm, and 0.198 nm, respectively. Clearly, Nb has remarkable size difference with Co and Al, and this is favorable for the glass formation [1]. Furthermore, the mixing enthalpy is -25 kJ mol^{-1} for Co–Nb, $+4$ kJ mol^{-1}for Zr–Nb, and -18 kJ mol^{-1} for Al–Nb, respectively [26]. According to the first empirical rules of Inoue, the formation of glass becomes easier with increasing the number of components in the alloy system. Therefore, increasing the number of alloy components to four elements by minor addition of Nb increases the mixing entropy of the alloy system, and as a result, the formation of glass becomes easier [1, 27]. Indeed, the minor addition of Nb can improve the GFA of $(Zr_{56}Co_{28}Al_{16})_{98}Nb_2$ by stabilizing the liquid phase or destabilizing the competing crystalline phases during solidification. On the other hands, the addition of Nb makes the atomic mismatch larger in the material and increases local random packing density. Addition of an extra element (Nb) to a certain extent into the base alloy highlights the confusion principle and forbids the crystallization [28]. But the larger content of Nb in Nb-4 sample has deteriorated the GFA of $(Zr_{56}Co_{28}Al_{16})_{96}Nb_4$ (see Table 1).

The other analysis which can be extracted from DSC signals in Fig. 2a is the sub-T_g structural relaxation in the

prepared samples. When as-cast MG samples are heated within the DSC instrument, they show a broad exothermic spectrum preceding the glass transition (see specific heat exotherms in Fig. 3). The relaxation enthalpy (ΔH_{rel}), which is a quantitative indication for the internal energy of MG [29, 30], can be calculated by integrating from the heat exotherms in Fig. 3 using the following equation [6]:

$$\Delta H_{rel} = \int_{T_{onset}}^{T_g} \Delta C_p dT \quad (1)$$

where T_{onset} is the onset temperature of relaxation, and C_p is the specific heat capacity of the sample.

As can be seen from Fig. 3, the specific heat capacity curves become narrower as the Nb content is increased. The calculated values of ΔH_{rel} for Nb-0, Nb-2, and Nb-4 samples are, respectively, 11.06, 8.35, and 2.83 J g^{-1}. This finding implies that the minor additions of Nb to the $Zr_{56}Co_{28}Al_{16}$ alloy significantly reduce the internal energy of MG and bring the glass to more relaxed states (i.e., lower ΔH_{rel}). A previous study also shows that the cerium and iron traces in La–Al–Ni MG rods reduce ΔH_{rel} by ~ 10% [31].

Figure 4 shows the quasi-static stress–strain curves of the BMG samples. It is evident from Fig. 4 that Nb-2 sample has the best mechanical properties in terms of the compressive strength and plasticity. The values of ultimate compressive strength (σ_u) and plastic strain (ε_p) determined from the stress–strain curves (Fig. 4) are summarized in Table 2. The amount of σ_u in Nb-2 reaches ~ 2.5 GPa, which is 21% larger than Nb-0 sample (σ_u of ~ 2.1 GPa). Further, ε_p significantly increases from ~ 1.11% in Nb-0 sample to ~ 6% in Nb-2 sample. In addition, the value of ε_p in Nb-4 (~ 2.1%) is also larger than Nb-0 sample. It is to be noted that the values of σ_u and ε_p achieved for

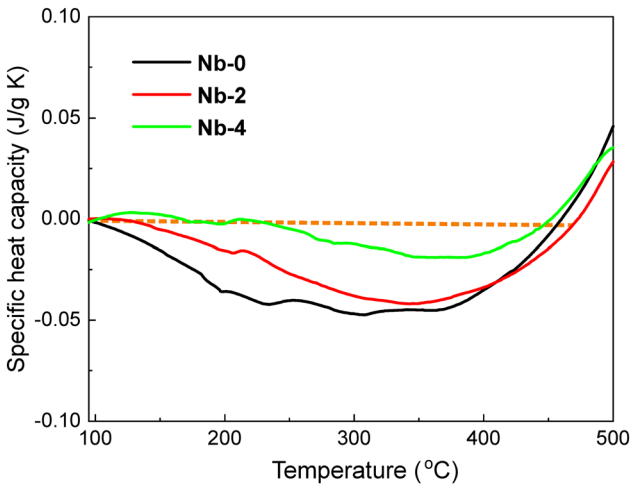

Fig. 3 DSC signals for Nb-0, Nb-2, and Nb-4 samples, highlighting the sub-Tg structural relaxation

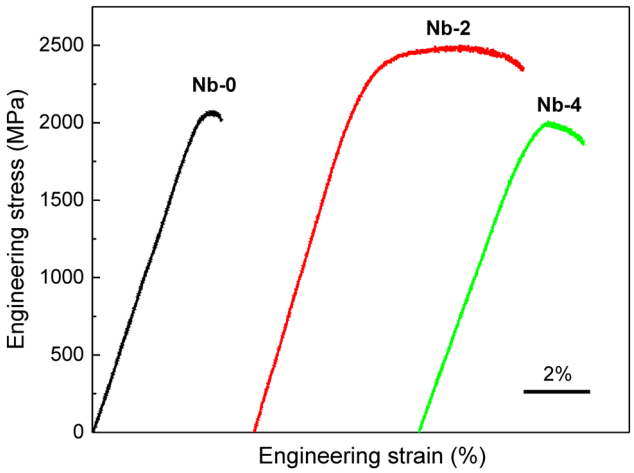

Fig. 4 The quasi-static stress–strain curves of as-cast samples

Table 2 The quasi-static compressive test results of BMG samples

Sample	σ_u (MPa)	ε_p (%)
Nb-0	2073 ± 80	1.11 ± 0.25
Nb-2	2500 ± 60	6 ± 1.20
Nb-4	2008 ± 50	2.1 ± 0.50

$Zr_{56}Co_{28}Al_{16}Nb_2$ BMG in this study are larger than the previous data reported for the microalloyed $Zr_{56}Co_{28}Al_{16}$ BMGs [18, 23, 32]. This fact highlights the key role of optimum minor alloying (type and amount of doped element) on the enhancement of mechanical properties in Zr-based BMGs.

As mentioned before, while Co–Nb and Al–Nb have negative mixing enthalpies, the mixing enthalpy of Zr–Nb is + 4 kJ mol^{-1}, and this large difference in mixing enthalpies may cause chemical heterogeneities which further lead to different local atomic packing and hard and soft atomic regions. Since the shear band formation is a heterogeneous nucleation process initiating on 3 regions and is restricted to propagation by the surrounding harder regions. The interaction of the shear bands with the hard region may cause different phenomena such as shear band deflection and branching. Consequently, the strength and ductility of BMG will be improved [27].

Figure 5 shows the overall view of the fractured samples after the quasi-static compressive test. As can be seen from Fig. 5, the fracture angles in Nb-0 and Nb-2 samples are 43.36° and 40.54°, respectively. It is worthy to note that the larger fracture angle (closer to 45° in Zr-based BMGs) reflects higher plasticity and improved mechanical performance in BMGs [9], and this is in line with our mechanical properties results (Fig. 4, Table 2) that Nb-2 has higher ε_p as compared to Nb-0 sample. The fracture angle is related

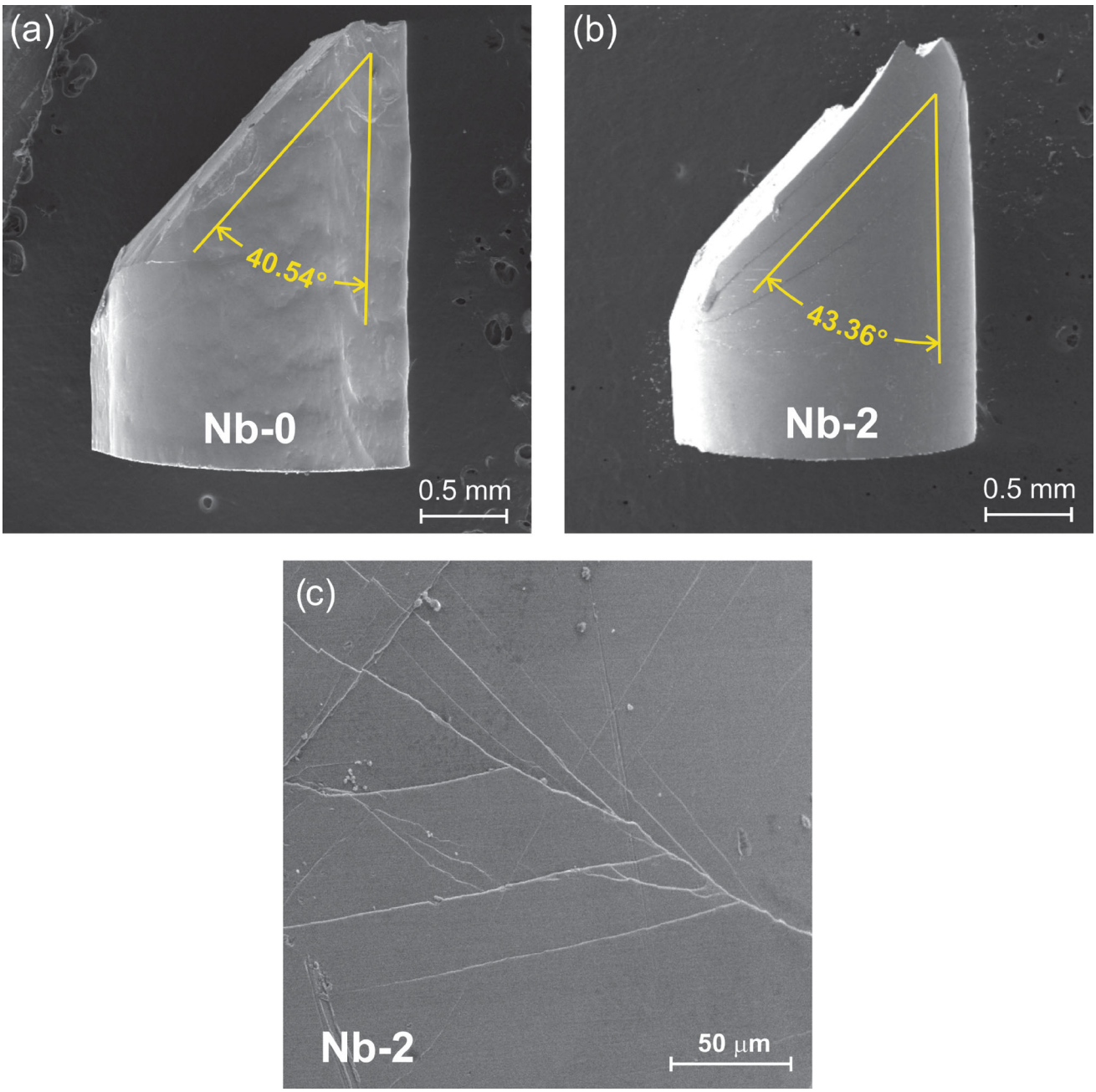

Fig. 5 The SEM micrographs for as-cast Nb-0 and Nb-2 samples. **a**, **b** An overall view of fractured samples. **c** Shear band propagation and branching in Nb-2 sample

to the rotation mechanisms of the primary shear band. At the early stage of deformation, primary shear bands form at the maximum shear plane (inclined at 45° with respect to the loading direction). As larger deformation is imposed on the sample, secondary shear bands are activated which can strongly interact with the primary shear bands. With the increase in the plastic deformation, a strong impingement is created between the primary and secondary shear bands, yielding a shear step on a shear plane as well as a rotation of the primary shear band towards the horizontal direction of the specimen. Therefore, the fracture angle of the sample having larger ε_p is closer to 45° [9, 33, 34].

It is also evident from Fig. 5a, b that while no shear banding is observed for Nb-0 sample on the peripheral surface (normal to the fracture surface), at least two primary shear bands are obvious for Nb-2 sample. In addition, the SEM image at higher magnification for Nb-2 sample (Fig. 5c) clearly shows that the branching of shear bands as well as shear band multiplication occurs in this sample. Hence, the large plasticity observed in Nb-2 sample can be

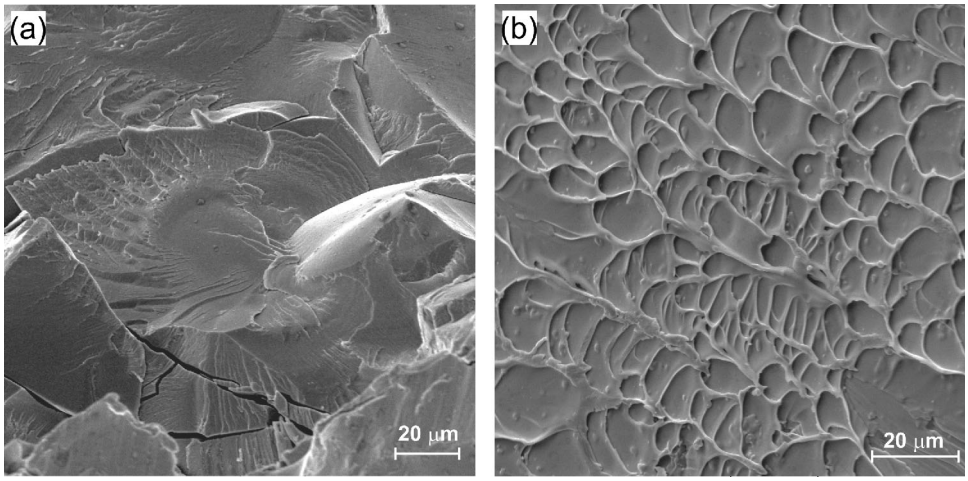

Fig. 6 The SEM micrographs of fracture surface for **a** Nb-0 and **b** Nb-2 samples

attributed to the propagation and branching of the shear bands.

The SEM micrographs of the fracture surface for Nb-0 and Nb-2 samples are shown in Fig. 6. As can be detected, there are two main regions in the fracture surface. The first region is a vein-like pattern, being a typical fracture feature for BMGs that is formed from the local melting within the shear bands. The second region is the smooth pattern representing the brittle fracture [1, 9, 23, 35]. It is clear from Fig. 6a that Nb-0 sample has a smooth fracture morphology containing large cracks and few veins. However, a large density of vein-like pattern is observed for Nb-2 sample (Fig. 6b). These fracture morphologies in Nb-0 and Nb-2 samples well correlate with their mechanical response since the plasticity of BMG samples directly depends on the density of vein-like patterns in fracture surface [9, 34, 35].

4 Conclusions

The results of the present study showed that the best GFA and mechanical performance (σ_u of $\sim$ 2.5 GPa and ε_p of 6%) was achieved in $(Zr_{56}Co_{28}Al_{16})_{98}Nb_2$ BMG sample. Further, the existence of larger contents in Nb-4 sample deteriorated both the GFA and mechanical properties. The microscopic observations revealed the branching and multiplication of shear bands in Nb-2 sample. Also, the observation of large density of vein-like patterns in the fracture surface of Nb-2 confirmed the improvement of plasticity.

References

[1] Suryanarayana C, and Inoue A, *Bulk Metallic Glasses*, CRC Press, Boca Raton (2018).
[2] Tan J, Zhang Y, Stoica M, Kühn U, Mattern N, Pan F S, and Eckert J, *Intermetallics* **19** (2011) 567.
[3] Louzguine-Luzgin D V, Zadorozhnyy V Y, Ketov S V, Wang Z, Tsarkov A A, and Greer A L, *Acta Mater* **129** (2017) 343.
[4] Trexler M M, and Thadhani N N, *Prog Mater Sci* **55** (2010) 759.
[5] Chen S, Tu J, Wu J, Hu Q, Xie S, and Zou J, *Mater Sci Eng A* **656** (2016) 84.
[6] Sun Y, Concustell A, and Greer A L, *Nat Rev Mater* **1** (2016) 16039.
[7] Hua N, and Chen W, *J Alloys Compd* **693** (2017) 816.
[8] Li T H, Liao Y C, Song S M, Jiang Y L, Tsai P H, Jang J S C, and Huang J C, *Intermetallics* **93** (2018) 162.
[9] Farahani F, and Gholamipour R, *Mater Sci Eng A* **651** (2016) 968.
[10] Nollmann N, Binkowski I, Schmidt V, Rösner H, and Wilde G, *Scr Mater* **111** (2016) 119.
[11] Qiao J C, Yao Y, Pelletier J M, Keer L M, *Int J Plast* **82** (2016) 62.
[12] Ren H T, Pan J, Chen Q, Chan K C, Liu Y, Liu L, *Scr Mater* **64** (2011) 609.
[13] Li H F, and Zheng Y F, *Acta Biomater* **36** (2016) 1.
[14] Qiang J, and Tsuchiya K, *J Alloys Compd* **712** (2017) 250.
[15] Liu G Q, Kou S Z, Li C Y, Zhao Y C, and Suo H L, *Trans Nonferrous Met Soc China* **22** (2012) 590.
[16] Mahmoodan M, Gholamipour R, Mirdamadi S, and Nategh S, *J Mater Eng Perform* **26** (2017) 5571.
[17] Wang R, Wang Y, Ang Y J, Sun J, and Xiong L, *J Non-Cryst Solids* **411** (2015) 45.
[18] Rahvard M M, Tamizifar M, and Boutorabi M A, *J Non-Cryst Solids* **491** (2018) 114.
[19] Dong Q, Pan Y J, Tan J, Qin X M, Li C J, Gao P, Feng Z X, and Calin M, *J Alloys Compd* **785** (2019) 422.
[20] Dechuan Y, Xue L, Xiaoyu W, and Shengli L, *Mater Lett* **234** (2019) 291.
[21] Hua N, Huang L, Wang J, Cao Y, He W, Pang S, and Zhang T, *J Non-Cryst Solids* **358** (2012) 1599.
[22] Zhang C, Li N, Pan J, Guo S F, Zhang M, and Liu L, *J Alloys Compd* **504** (2010) 163.
[23] Rahvard M M, Tamizifar M, and Boutorabi S M, *Trans Nonferrous Met Soc China* **28** (2018) 1543.

[24] Kuball A, Gross O, Bochtler B, Adam B, Ruschel L, Zamanzade M, and Busch R, *J Alloys Compd* **790** (2019) 337.
[25] Waniuk T A, Schroers J, and Johnson W L, *Appl Phys Lett* **78** (2001) 1213.
[26] Takeuchi A, and Inoue A, *Metall Mater Trans* **46** (2005) 2817.
[27] Rashidi R, Malekan M, and Gholamipour R, *Mater Sci Eng A* **729** (2018) 433.
[28] Inoue A, *Acta Mater* **48** (2000) 279.
[29] Ketov S V, Sun Y H, Nachum S, Lu Z, Checchi A, Beraldin A R, Bai H Y, Wang W H, Louzguine-Luzgin D V, Carpenter M A, and Greer A L, *Nature* **524** (2015) 200.
[30] Sohrabi S, Li M X, Bai H Y, Ma J, Wang W H, and Greer A L, *Appl Phys Lett* **116** (2020) 081901.
[31] Sohrabi S, Ri M C, Jiang H Y, Gu L, Wen P, Sun Y H, and Wang W H, *Intermetallics* **111** (2019) 106497.
[32] Zhang T, and Inoue A, *Metall Mater Trans* **43** (2002) 267.
[33] Chen C, Gao M, Wang C, Wang W, and Wang T, *Sci Rep* **6** (2016) 39522.
[34] Zhang Z F, He G, Zhang H, and Eckert J, *Scr Mater* **52** (2005) 945.
[35] Mahmoodan M, Gholamipour R, Mirdamadi S, and Nategh S, *Metall Mater Trans A* **48** (2017) 2496.